

Supporting Information

Vertically aligned 1T-2H MoS₂ on 3D porous carbon for ultrahigh-performance flexible energy storage device

Zhao Wang^{a,b,c}, Zongwei Guo^{a,b,c}, Jiajun Luo^{a,b,c}, Xuesong Wang^d, Ming Li^{a,b,c*},
Yuhui Ao^{a,b,c*} and Lin Jin^{a,b,c*}

^aCollege of Chemistry and Life Sciences, Changchun University of Technology, 2055 Yanan Street, Changchun, 130012, P. R. China

^bJilin Provincial Laboratory of Carbon Fiber and Composites, 2055 Yanan Street, Changchun, 130012, P. R. China

^cJilin Provincial Key Laboratory of Carbon Fiber Development and Application, 2055 Yanan Street, Changchun, 130012, P. R. China

^dDepartment of Chemistry, Northeast Normal University, 5268 Renmin Street, Changchun, 130012, P. R. China

Characterization

X-ray diffraction (XRD) was applied on a Bruker X-ray diffraction with Cu K α radiation ($\lambda = 1.54178 \text{ \AA}$) to determine the crystal phase of the synthesized products. The surface microstructure and composition of electrode materials were analyzed by field-emission scanning (FE-SEM) (JEOL7610, Japan). The surface chemical composition and structure were investigated by an X-ray photoelectron spectroscope (XPS) equipped with a monochromatic Al K α X-ray source operating at 100 W. Aberration-corrected scanning transmission electron microscopy

images were obtained on a JEM 2100 F/FEI probe-corrected transmission electron microscope (TEM). All DFT calculations are performed using the density functional theory method in the VASP package.

Electrochemical measurements

All electrochemical measurements, including constant current charge/discharge (GCD), cyclic voltammetry (CV), and electrochemical impedance spectroscopy (EIS), is completed on the electrochemical workstation (CH Instrument 760E). Electrode material characterizations were evaluated by a three-electrode system. The synthetic material was used as a working electrode, while platinum and Ag/AgCl tablets were used as the counter and reference electrodes, and a 3 M KOH aqueous solution was used for electrolysis. 1T-2H MS@BNC/CC//AC/CC was evaluated by a two-electrode system. Hydrogel is prepared by PVA and KOH as a gel electrolyte.

All specific capacitance is calculated based on eq S1.

$$C = j \Delta t / m \Delta V \quad (1)$$

Where C (F g⁻¹) is the specific capacitance, Δt (s) is the discharge time, j is the current density, m (g) is the effective mass, and ΔV (V) is the potential window.

The measurement of current *i* mainly consists of two parts: diffusion control (*i_{diff}*) and capacitance control (*i_{cap}*), which can be represented by eq S2 and S3.

$$i = i_{diff} + i_{cap} \quad (2)$$

$$i = a V^b \quad (3)$$

Among them, *v* is the scanning rate, and *a* and *b* are the fitting parameters obtained by log*i* regarding log*v*. The control process can be analyzed through the *b*

value. When the b value approaches 0.5, the dynamic mechanism of the electrode is diffusion control, and when the b value approaches 1, it is surface capacitance control.

The quantification of the capacitance contribution rate is calculated according to eq S4.

$$i(V) = k_1 v + k_2 v^{1/2} \quad (4)$$

Where i is the response current at the potential of V , $k_1 v$ and $k_2 v^{1/2}$ represent the contributions of surface control processes and diffusion control processes, respectively

The energy density and power density Were calculated using eq S5 and S6, respectively.

$$E = C * \Delta V^2 / (2 * 3.6) \quad (5)$$

$$P = 3600 E / \Delta t \quad (6)$$

Where the energy density and power density are E (Wh kg^{-1}) and P (W kg^{-1}), respectively, C (F g^{-1}) is the specific capacitance, ΔV (V) is the potential window, and Δt (s) is the discharge time.

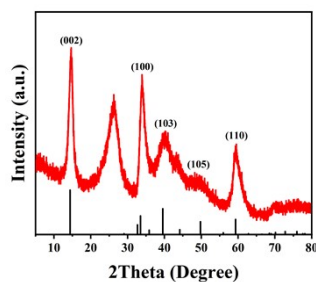


Figure S1. XRD spectra of MS/CC

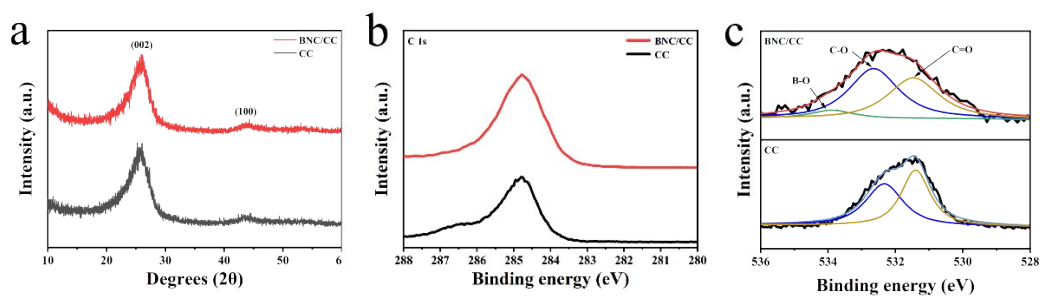


Figure S2. (a) XRD spectra of BNC/CC, and CC. (b) XPS analysis of the C 1s region of BNC/CC and CC. (c) XPS analysis of the O 1s region of as-synthesized BNC/CC and CC.

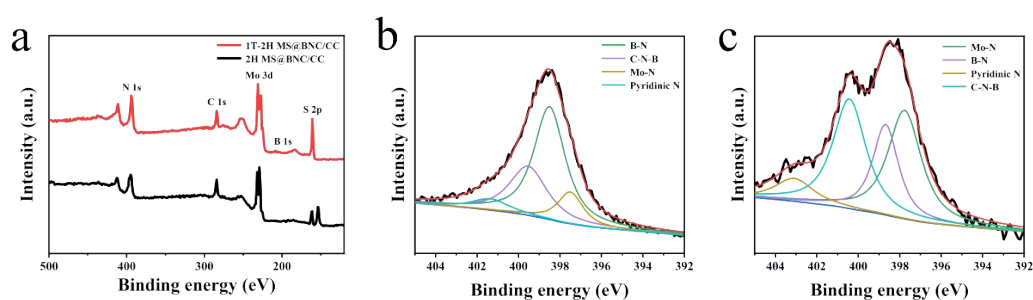


Figure S3. (a) Comparison of XPS spectra between 2H MS@BNC/CC and 1T-2H MS@BNC/CC. (b) XPS analysis of the N 1s region of as-synthesized 2H MS@BNC/CC samples. (c) XPS analysis of the N 1s region of as-synthesized 1T-2H MS@BNC/CC samples.

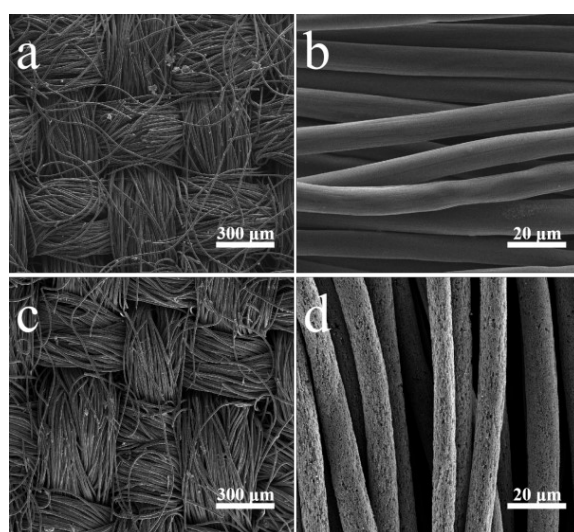


Figure S4. (a, b) SEM images of CC. (c, d) SEM images of BNC/CC.

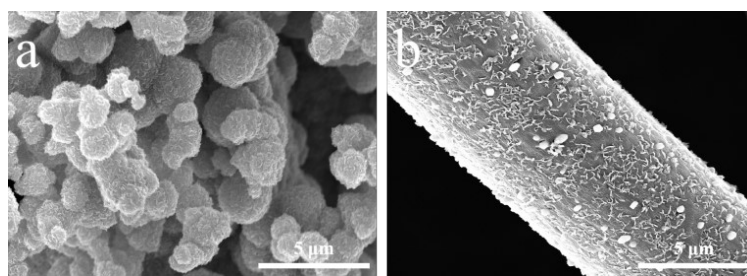


Figure S5. (a) SEM images of MS/CC. (d) SEM images of 2H MS@BNC/CC.

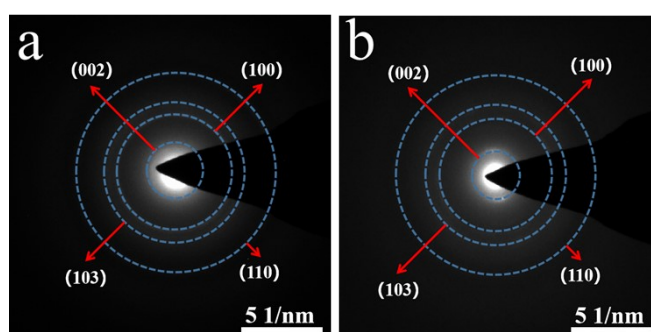


Figure S6. (a) SAED pattern of 2H MS@BNC/CC. (b) SAED pattern of 1T-2H MS@BNC/CC

Table S1. Comparison of electrochemical performance between 1T-2H MS@BNC/CC and reported MoS₂ based supercapacitors

Electrode materials	Electrolyte	Specific capacitance (F g ⁻¹)	Reference
1T-2H MS@BNC/CC	3 M KOH	994.28 at 0.5 A g ⁻¹	This work
MoS ₂ /C	1 M KOH	589 at 0.5 A g ⁻¹	1
MoS ₂ /PANI	1 M H ₂ SO ₄	521.7 at 1 A g ⁻¹	3
MoS ₂ Nanoflower	3 M KOH	368 at 1 A g ⁻¹	4
PANI/MoS ₂ - MnO ₂	1 M KOH	469 at 1 A g ⁻¹	5
MoS ₂ /PANI-53	1 M H ₂ SO ₄	476 at 0.5 A g ⁻¹	6
MoS ₂ /PPy	1 M KOH	654 at 1 A g ⁻¹	7
MoS ₂ -Gr	1 M Na ₂ SO ₄	243 at 1 A g ⁻¹	8
MoS ₂ /rGO/PANI	1 M H ₂ SO ₄	570 at 1 A g ⁻¹	9
MoS ₂ nanoworms	1 M Na ₂ SO ₄	138 at 1 A g ⁻¹	10

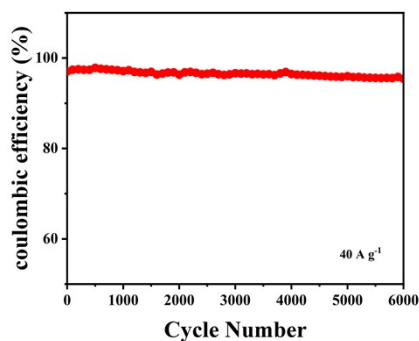


Figure S7. Coulombic efficiency during 6000 cycles for the 1T-2H MS@BNC/CC electrode at 40 A g^{-1} .

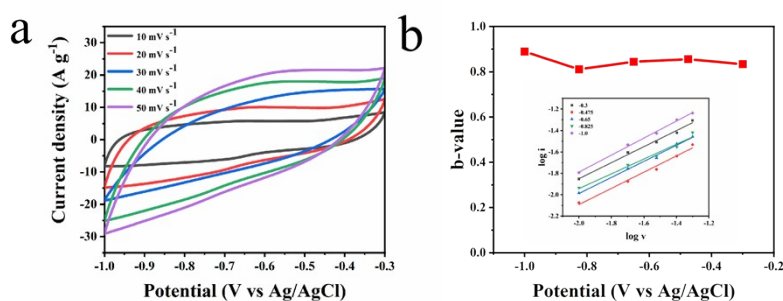


Figure S8. (a) CV curves of 1T-2H MS@BNC/CC at 10-50 mV s^{-1} . (b) The b values for the 1T-2H MS@BNC/CC; the inset shows the current response vs. the scan rate for 1T-2H MS@BNC/CC at different voltages.

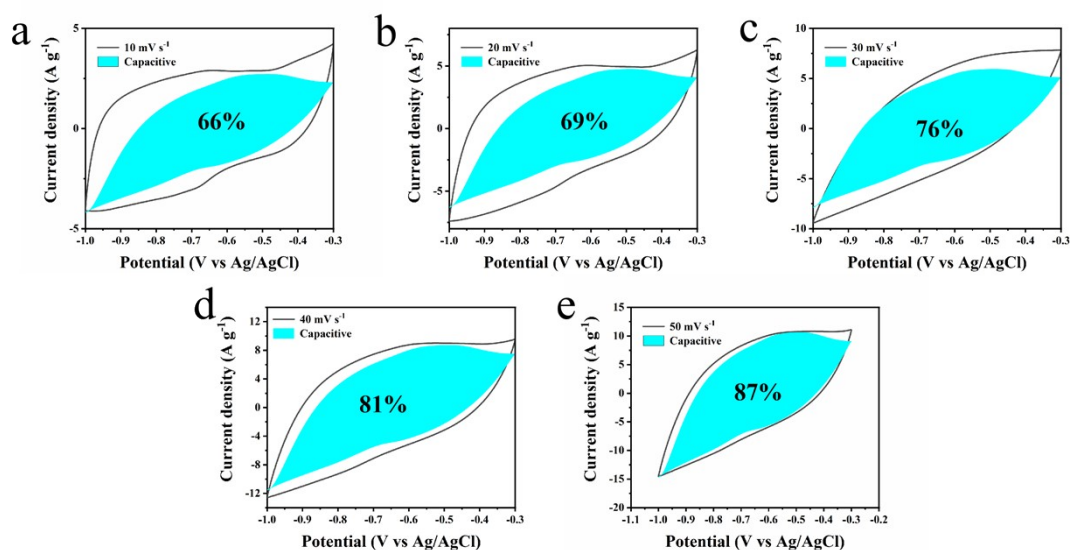


Figure S9. CV partition analysis showing the capacitive contribution to the total current at selected

scan rates. (a) 10 mV s⁻¹. (b) 20 mV s⁻¹. (c) 30 mV s⁻¹. (d) 40 mV s⁻¹. (e) 50 mV s⁻¹.

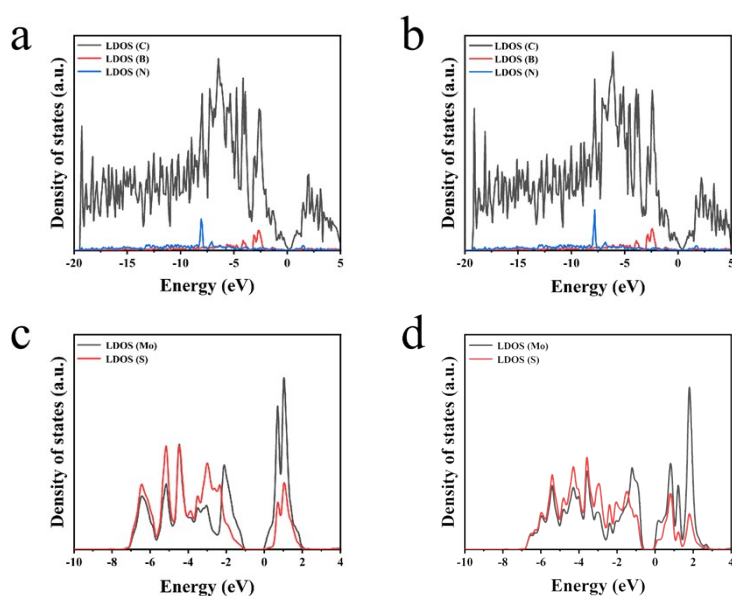


Figure S10. (a) LDOS distribution of C, N, and B in 2H MS@BNC/CC. (b) LDOS distribution of C, N, and B in 1T-2H MS@BNC/CC. (c) LDOS distribution of Mo and S in 2H MS@BNC/CC. (d) LDOS distribution of Mo and S in 1T-2H MS@BNC/CC.

Table S2. Comparison of electrochemical performance between 1T-2H MS@BNC/CC and reported MoS₂ based supercapacitors

Electrode materials	Electrolyte	Energy density (Wh·kg ⁻¹)	Power density (W·kg ⁻¹)	Reference
1T-2H MS@BNC/CC	KOH	92.285	349.7	This work
MoS ₂ /NiS	KOH	31	155.7	2
PANI/MoS ₂ -MnO ₂	KOH	35.97	500	5
MoS ₂ /PANI-53	H ₂ SO ₄	35	335	6
MoS ₂ /PPy	KOH	66	488	7
Co ₉ S ₈ /α-MnS@N-C@MoS ₂	KOH	64.2	729.2	11
PAN/MoO ₂ /MoS ₂	KOH	46	2246.9	12
MoS ₂ @3DGN	KOH	36.43	400	13
NMS/CNT	KOH	40	400	14

References

- (1) Ji, H.; Liu, C.; Wang, T.; Chen, J.; Mao, Z.; Zhao, J.; Hou, W.; Yang, G., Porous Hybrid Composites of Few-Layer MoS₂ Nanosheets Embedded in a Carbon Matrix with an Excellent Supercapacitor Electrode Performance. *Small* **2015**, 11 (48), 6480-90.
- (2) Qin, Q.; Chen, L.; Wei, T.; Liu, X., MoS₂/NiS Yolk-Shell Microsphere-Based Electrodes for Overall Water Splitting and Asymmetric Supercapacitor. *Small* **2019**, 15 (29), e1803639.
- (3) Dai, J.; Zeng, S.; Lv, Y.; Xie, H.; Luo, L.; Xu, Y.; Dai, L., A facile strategy for tailoring polyaniline by MoS₂ nanosheets to obtain excellent electrochemical properties. *Electrochimica Acta* **2021**, 378.
- (4) Javed, M. S.; Dai, S.; Wang, M.; Guo, D.; Chen, L.; Wang, X.; Hu, C.; Xi, Y., High performance solid state flexible supercapacitor based on molybdenum sulfide hierarchical nanospheres. *Journal of Power Sources* **2015**, 285, 63-69.
- (5) Heydari, H.; Abdouss, M.; Mazinani, S.; Bazargan, A. M.; Fatemi, F., Electrochemical study of ternary polyaniline/MoS₂-MnO₂ for supercapacitor applications. *Journal of Energy Storage* **2021**, 40.
- (6) Ren, L.; Zhang, G.; Lei, J.; Hu, D.; Dou, S.; Gu, H.; Li, H.; Zhang, X., Growth of PANI thin layer on MoS₂ nanosheet with high electro-capacitive property for symmetric supercapacitor. *Journal of Alloys and Compounds* **2019**, 798, 227-234.

- (7) Niaz, N. A.; Shakoor, A.; Imran, M.; Khalid, N. R.; Hussain, F.; Kanwal, H.; Maqsood, M.; Afzal, S., Enhanced electrochemical performance of MoS₂/PPy nanocomposite as electrodes material for supercapacitor applications. *Journal of Materials Science: Materials in Electronics* **2020**, 31 (14), 11336-11344.
- (8) Huang, K.-J.; Wang, L.; Liu, Y.-J.; Liu, Y.-M.; Wang, H.-B.; Gan, T.; Wang, L.-L., Layered MoS₂-graphene composites for supercapacitor applications with enhanced capacitive performance. *International Journal of Hydrogen Energy* **2013**, 38 (32), 14027-14034.
- (9) Bai, L. Z.; Wang, Y. H.; Cheng, S. S.; Li, F.; Zhang, Z. Y.; Liu, Y. Q., Synthesis and Electrochemical Performance of Molybdenum Disulfide-Reduced Graphene Oxide-Polyaniline Ternary Composites for Supercapacitors. *Front Chem* **2018**, 6, 218.
- (10) Neetika; Sanger, A.; Malik, V. K.; Chandra, R., One step sputtered grown MoS₂ nanoworms binder free electrodes for high performance supercapacitor application. *International Journal of Hydrogen Energy* **2018**, 43 (24), 11141-11149.
- (11) Kandula, S.; Shrestha, K. R.; Kim, N. H.; Lee, J. H., Fabrication of a 3D Hierarchical Sandwich Co₉S₈/alpha-MnS@N-C@MoS₂ Nanowire Architectures as Advanced Electrode Material for High Performance Hybrid Supercapacitors. *Small* **2018**, 14 (23), e1800291.
- (12) Mu, J.; Guan, Y.; Wang, L.; Li, H.; Liu, Y.; Che, H.; Liu, A.; Guo,

- Z.; Zhang, X.; Zhang, Z., Flexible heat-treated PAN nanofiber/MoO₂/MoS₂ composites as high performance supercapacitor electrodes. *Journal of Materials Science: Materials in Electronics* **2019**, 30 (9), 8210-8219.
- (13) Zhou, R.; Han, C.-j.; Wang, X.-m., Hierarchical MoS₂-coated three-dimensional graphene network for enhanced supercapacitor performances. *Journal of Power Sources* **2017**, 352, 99-110.
- (14) Yang, X.; Zhao, L.; Lian, J., Arrays of hierarchical nickel sulfides/MoS₂ nanosheets supported on carbon nanotubes backbone as advanced anode materials for asymmetric supercapacitor. *Journal of Power Sources* **2017**, 343, 373-382.